

Empirical Constraints on the First Stars and Quasars

Z. Haiman[†] and A. Loeb^{*}

[†]*Astrophysics Theory Group, Fermi National Accelerator Laboratory, Batavia, IL 60510*

^{*}*Harvard-Smithsonian Center for Astrophysics, 60 Garden Street, Cambridge, MA 02138*

Abstract. Empirical studies of the first generation of stars and quasars in the Universe will likely become feasible over the next decade. The *Next Generation Space Telescope* will provide direct imaging and photometry of sub-galactic objects at $z \gtrsim 10$, while microwave anisotropy experiments, such as MAP or Planck, will set constraints on the ionization history of the intergalactic medium due to these sources. We describe the expected signals that will be detectable with these future instruments.

INTRODUCTION

The cosmic dark age [1] ended when the first gas clouds condensed out of the primordial fluctuations at redshifts $z = 10 - 20$ [2]. These condensations gave birth to the first star-clusters or mini-quasars in the Universe. Previous observations have not yet probed this epoch. Existing optical or infrared telescopes are capable of reaching out to redshifts $z \lesssim 6$, while current anisotropy experiments of the cosmic microwave background (CMB) probe only the recombination epoch at $z \sim 10^3$. The remaining observational gap between these redshift regimes is likely to be bridged over the coming decade. In particular, the planned launch of the infrared Next Generation Space Telescope (NGST) will enable direct imaging of sub-galactic objects at $z \gtrsim 10$, while microwave anisotropy satellites such as MAP or Planck will measure complementary signatures from the reionization of the intergalactic medium at these redshifts.

The detection [3,4] of Ly α emission from galaxies at redshifts up to $z = 5.7$ demonstrates that reionization due to the first generation of sources must have occurred at yet higher redshifts; otherwise, the damping wing of Ly α absorption by the neutral intergalactic medium would have eliminated the Ly α line in the observed spectrum of these sources [5,6]. In this review, we predict the redshift of reionization in popular cosmological models, and estimate the signals from this epoch that will become detectable with the NGST, MAP, or the Planck satellites.

PROPERTIES OF THE FIRST OBJECTS

The first objects left behind a variety of fossil evidence of their existence [7], including the enrichment of the intergalactic medium (IGM) with heavy elements, the reionization of the IGM, the distortion of the CMB spectrum by dust-processed radiation [8], and the production of stellar remnants. In the following, we explore the signatures of the early stars and mini-quasars using a simple semi-analytical model, based on the Press-Schechter formalism [9]. We calibrate the total amount of light that stars or mini-quasars produce based on data from redshifts $z \lesssim 5$. The efficiency of early star formation is calibrated based on the observed metallicity of the intergalactic medium [10,11], while the early quasars are constrained so as to match the quasar luminosity function [12] at redshifts $z \lesssim 5$, as well as data from the Hubble Deep Field (HDF) on faint point-sources. We focus on a particular cosmological model with a cosmological constant, $(\Omega_0, \Omega_\Lambda, \Omega_b, h, \sigma_{8h^{-1}}, n) = (0.35, 0.65, 0.04, 0.65, 0.87, 0.96)$, named the “concordance model” by Ostriker & Steinhardt [13]. For a discussion of other cosmological models, as well as a more detailed description of our methods and results, we refer the reader to several papers [26,14–20]. More advanced 3-D numerical simulations have only now started to address the complicated physics associated with the fragmentation, chemistry, and radiative transfer of the primordial molecular clouds [21], as well as with the reionization of the IGM [22].

Following collapse, the gas in the first baryonic condensations is virialized by a strong shock [23]. The shock-heated gas can only continue to collapse and fragment if it cools on a timescale shorter than the Hubble time. In the metal-poor primordial gas, the only coolants that satisfy this requirement [24] are neutral atomic hydrogen (H) and molecular hydrogen (H_2). However, H_2 molecules are fragile, and are easily photo-dissociated throughout the universe by trace amounts of starlight [25,26] that are well below the level required for complete reionization of the Universe. Hence, most of the sources that ionized the Universe formed inside objects with virial temperatures $T_{\text{vir}} \gtrsim 10^4\text{K}$, or masses $\sim 10^8 M_\odot$, which cooled via atomic transitions. Depending on the details of their cooling and angular momentum transport, the gas in these objects fragmented into stars, or formed a central black hole exhibiting quasar activity. Although the first objects contained only a small fraction of the total mass of the universe, they could have had a dramatic effect on the subsequent evolution of the ionization and temperature of the rest of the gas [27]. Since nuclear fusion releases ~ 7 MeV per baryon, and accretion onto a black hole may release even more energy, and since the ionization of a hydrogen atom requires only 13.6 eV, it is sufficient to convert a small fraction of the baryonic mass into either stars or black holes in order to ionize the rest of the Universe.

The cooling gas clouds eventually fragment into stars [28]. Although the actual fragmentation process is likely to be rather complex, the average fraction f_{star} of the collapsed gas converted into stars can be calibrated empirically so as to reproduce the average metallicity observed in the Universe at $z \approx 3$. For the purpose of this calibration, we use the average C/H ratio, inferred from CIV absorption lines in Ly α forest clouds [10,11]. The observed ratio is between 10^{-3} and 10^{-2} of the solar

value [29]. If the carbon produced in the early star clusters is uniformly mixed with the rest of the baryons in the Universe, this implies $f_{\text{star}} \approx 2\text{--}20\%$ for a Scalo [30] stellar mass function. This number assumes inefficient hot bottom burning, i.e. maximal carbon yields [31], and includes a factor of ~ 3 due to the finite time required to produce carbon inside the stars (in a Press–Schechter star formation history, only a third of the total stellar carbon yield is produced and ejected by $z = 3$). Ultimately, 3-D simulations of the first generation of stars might be used to infer the expected star–formation efficiency in the first generation of gas clouds. Preliminary runs [32] imply that $\sim 1\%$ of the gas condenses into dense cores which could yield massive stars.

An even smaller fraction of the cooling gas might condense at the center of the potential well of each cloud and form a massive black hole, exhibiting mini–quasar activity. In the simplest scenario we postulate that the peak luminosity of each black hole is proportional to its mass, and there exists a universal quasar light–curve in Eddington units. This hypothesis is motivated by the fact that for a sufficiently high fueling rate, quasars are likely to shine at their maximum possible luminosity, which is some constant fraction of the Eddington limit, for a time which is dictated by their final mass and radiative efficiency. Allowing the final black hole mass M_{bh} to be a fixed fraction of the total halo mass M_{halo} , we find that there exists a universal light curve [$L(t) = L_{\text{Edd}} \exp(-t/t_0)$, with $t_0 \sim 10^6$ yr], for which the Press–Schechter theory provides an excellent fit to the observed evolution of the luminosity function (LF) of bright quasars between redshifts $2.6 < z < 4.5$. The required black hole to halo gas mass ratio is $M_{\text{bh}}/M_{\text{gas}} = 10^{-3.2}\Omega_0/\Omega_b = 5.5 \times 10^{-3}$, close to the typical value of $\sim 6 \times 10^{-3}$ found for the ratio of black hole mass to spheroid mass in a dozen nearby galaxies [33,34]. The existence of massive black holes in the centers of low–mass galaxies such as M32 or NGC 4486B [33,34] implies that the process of black hole formation does not discriminate against galaxies of this type. Since galaxies at $z \sim 10$ have a similar mass and velocity dispersion as these low–redshift examples, it is conceivable that low–luminosity quasars contributed significantly to the reionization of the Universe.

One does expect, however, that the ratio $M_{\text{bh}}/M_{\text{gas}}$ would have a substantial intrinsic scatter. Observationally, the scatter around the average value of $\log(M_{\text{bh}}/L)$ is 0.3 [34], while the standard deviation in $\log M_{\text{bh}}/M_{\text{gas}}$ has been found to be $\sigma \sim 0.5$ [35]. Such an intrinsic scatter would flatten the predicted quasar LF at the high mass end, where the LF is a steep function of black hole mass. As an illustrative example, we show in Figure 1 the mass function of black holes in the Press–Schechter model of halos, with or without this scatter (solid versus short-dashed lines). In order to eliminate the flattening introduced by the scatter, we find that the average black hole to halo mass ratio must be reduced by $\sim 50\%$. The dot–dashed line in Figure 1 demonstrates that such a reduction would indeed compensate for the effect of an intrinsic scatter in the relevant mass range ($10^8 M_{\odot} \lesssim M_{\text{bh}} \lesssim 10^{10} M_{\odot}$). Figure 1 also shows the effect of a more significant intrinsic scatter ($\sigma \sim 1$) on the black hole mass function (long-dashed lines). We find that the predicted black hole mass function in the presence of such a large

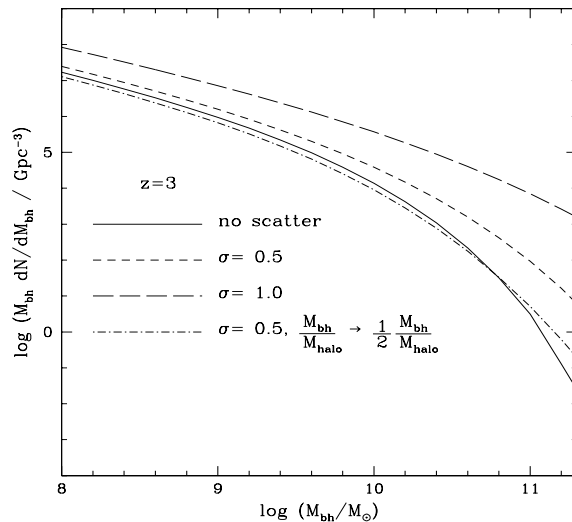


FIGURE 1. The comoving mass function of black holes at redshift $z = 3$ when a scatter is introduced to the logarithm of the ratio between the black hole and halo masses, $\log(M_{\text{bh}}/M_{\text{halo}})$.

scatter would be significantly different from any model with a constant value for $M_{\text{bh}}/M_{\text{gas}}$.

In reality, the relation between the black hole and halo masses may be more complicated than linear in reality. With the introduction of additional free parameters, a non-linear (mass and redshift dependent) relation between the black-hole and halo masses can also lead to acceptable fits [36] of the observed quasar LF. The nonlinearity in the relation must be related to the physics of the formation process of low-luminosity quasars, which was discussed in several papers [36–38]. If the black hole formation efficiency decreases in smaller halos, this would flatten the faint end of the LF, and therefore could not compensate the effect of a large intrinsic scatter of the type shown in Figure 1. Indeed, in order to fit the bright end of the LF in a model with a large intrinsic scatter, one must postulate that the black hole formation efficiency decreases in larger halos.

INFRARED NUMBER COUNTS

The Next Generation Space Telescope (*NGST*, [39]) will be able to detect the early population of star clusters and mini-quasars. *NGST* is scheduled for launch in 2007, and is expected to reach an imaging sensitivity of ~ 1 nJy (S/N=10 at spectral resolution $\lambda/\Delta\lambda = 3$) for extended sources after several hours of integration in the wavelength range of 1–3.5 μm . Figure 2 shows the predicted number counts in the models described above, normalized to a 5' \times 5' field of view. This figure shows

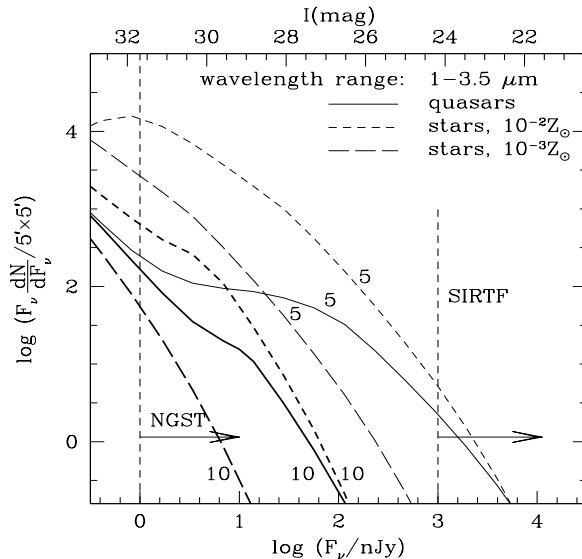


FIGURE 2. *Infrared Number Counts.* The solid curves refer to quasars, while the long/short dashed curves correspond to star clusters with low/high normalization for the star formation efficiency. The curves labeled “5” or “10” show the cumulative number of objects with redshifts above $z = 5$ or 10 .

separately the number per logarithmic flux interval of all objects with redshifts $z > 5$ (thin lines), and $z > 10$ (thick lines). The number of detectable sources is high; *NGST* will be able to probe about ~ 100 quasars at $z > 10$, and ~ 200 quasars at $z > 5$ per field of view. The bright-end tail of the number counts approximately follows a power law, with $dN/dF_\nu \propto F_\nu^{-2.5}$. The dashed lines show the corresponding number counts of “star-clusters”, assuming that each halo shines due to a starburst that converts a fraction of 2% (long-dashed) or 20% (short-dashed) of the gas into stars. These lines indicate that *NGST* would detect $\sim 40 - 300$ star-clusters at $z > 10$ per field of view, and $\sim 600 - 10^4$ clusters at $z > 5$. Unlike quasars, star clusters could in principle be resolved if they extend over a scale comparable to the virial radius of their dark matter halos [16]. The supernovae and γ -ray bursts in these star clusters might outshine their hosts and may also be directly observable [40,41].

CONSTRAINTS FROM THE HUBBLE DEEP FIELD

High resolution, deep imaging surveys can be used to set important constraints on semi-analytical models of the type described above. The properties of faint *extended* sources found in the Hubble Deep Field (HDF) [42] agree with detailed semi-analytic models of galaxy formation [43]. On the other hand, the HDF has revealed only a handful of faint *unresolved* sources, but none with the colors expected for high redshift quasars [44]. The simplest mini-quasar model described

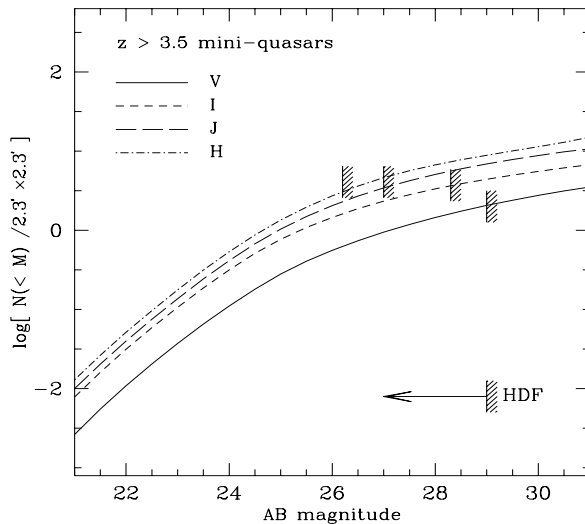


FIGURE 3. V , I , J , and H counts for mini-quasars in a model with a minimum halo circular velocity of $v_{\text{circ}} = 75 \text{ km s}^{-1}$. This model is consistent with HDF data in the V band at the 5% level. Sensitivities are shown in each band for the same signal-to-noise ratio and exposure time as the optical HDF.

above predicts the existence of ~ 10 B-band “dropouts” in the HDF, inconsistently with the lack of detection of such dropouts up to the $\sim 50\%$ completeness limit at $V \approx 29$ in the HDF. To reconcile the models with the data, a mechanism is needed for suppressing the formation of quasars in halos with circular velocities $v_{\text{circ}} \lesssim 50\text{--}75 \text{ km s}^{-1}$. This suppression naturally arises due to the photo-ionization heating of the intergalactic gas by the UV background after reionization [45,46]. Alternative effects could help reduce the quasar number counts, such as a change in the background cosmology, a shift in the “big blue bump” component of the quasar spectrum to higher energies due to the lower black hole masses in mini-quasars, or a nonlinear black hole to halo mass relation; however, these effects are too small to account for the lack of detections in the HDF [20].

The mini-quasars may not necessarily appear as point sources in the HDF if their extended host galaxies are actually resolved by *HST*. In fact, twelve candidate sources of activity in the nuclei of galaxies at high-redshifts ($z > 3.5$) have recently been identified [47] in the HDF. All of these point-like sources are embedded in extended host galaxies which are relatively bright ($V \sim 26\text{--}27$) and outshine their AGNs by typically 1 mag. As a consequence, these AGNs would have been missed by previous searches for isolated point-like sources [44]. In the models described above, the mini-quasars peak at a flux $\sim 1\text{--}3.5$ mag brighter in V than their host galaxy, which is assumed to undergo a starburst inside the same halo [18]. The twelve HDF candidates must reflect faint AGN activity in bright galaxies of relatively massive halos (analogous to a weak Seyfert activity), rather than faint

AGN activity in small halos as expected in our model. The observed sources might imply a phase in the history of massive halos that corresponds to an additional low-luminosity tail of the quasar lightcurve discussed above. An extended lightcurve would still be consistent with the luminosity function derived from the bright AGN phase and could explain the existence of the embedded AGNs in the HDF. The detection of faint embedded AGNs could also be related to the intrinsic scatter in the distribution of $M_{\text{bh}}/M_{\text{halo}}$ relation, and reflect objects with unusually small values of this mass ratio.

The longer infrared wavelengths, such as the J and H infrared bands, are better suited for studying the Universe at $z \gtrsim 5$. Forthcoming data on point-sources from NICMOS observations of the HDF [48] could improve the constraints on mini-quasar models. In Figure 3, we show the expected number counts of mini-quasars in the V , I , J , and H bands for the model which is consistent with the optical HDF data. The number of objects predicted in the I , J , and H bands is higher than in the optical HDF. The NICMOS data in these bands would either reveal several high redshift mini-quasars or else place tighter constraints on quasar models than currently possible using V and I data. With the post-reionization feedback on halos imposed by the optical HDF data, $v_{\text{circ}} \geq 75 \text{ km s}^{-1}$, we still expect at least ~ 5 mini-quasars to be found at $z > 3.5$ in the NICMOS J and H bands. A non-detection by NICMOS would translate to a minimum circular velocity of $v_{\text{circ}} \gtrsim 100 \text{ km s}^{-1}$, or a factor of ~ 2 increase in the low-mass cutoff for halos harboring quasars.

WAS THE UNIVERSE REIONIZED BY STARS OR MINI-QUASARS?

Given either the star-formation or quasar black-hole formation histories, we derive the reionization history of the IGM by following the radius of the expanding Strömgren sphere around each source. The reionization history depends on the time-dependent production rate of ionizing photons, their escape fraction, and the recombination rate of the IGM, which are all functions of redshift. The production rate of ionizing photons per quasar follows from the median quasar spectrum [49] and the light-curve we derived. The analogous rate per star follows from the time-dependent composite stellar spectrum, constructed from standard stellar atmosphere atlases [50] and evolutionary tracks [51]. We computed the escape fraction of ionizing photons in each halo, assuming ionization equilibrium inside an isothermal sphere where both the stars and the gas are distributed with a $1/r^2$ profile. For quasars, we assumed that the escape fraction is 100%. During reionization, we also assumed that the formation of low-mass halos is suppressed by photo-ionization heating inside the already ionized cosmological HII regions.

Figure 4 summarizes the resulting reionization histories from stars or quasars in our models with a Λ CDM cosmology. The results for stars are shown in two cases, one with $Z_{\text{IGM}} = 10^{-2}Z_{\odot}$ (dashed lines) and the other with $Z_{\text{IGM}} = 10^{-3}Z_{\odot}$

FIRST STARS AND QUASARS

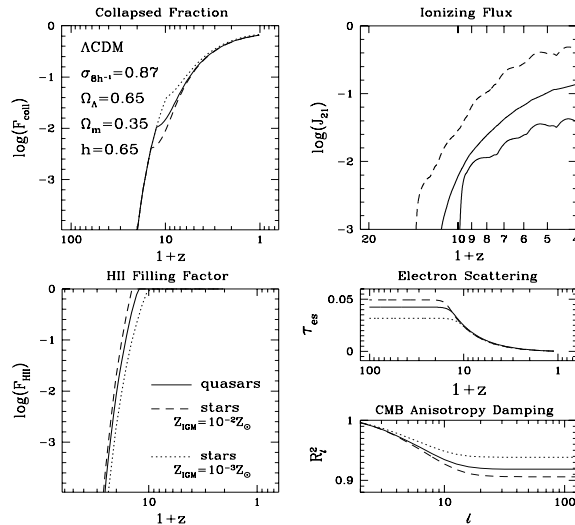


FIGURE 4. *Reionization history.* Clockwise, the different panels show: (i) the collapsed fraction of baryons; (ii) the background flux at the Lyman limit; (iii) the volume filling factor of ionized hydrogen; and (iv) the optical depth to electron scattering, and the corresponding damping factor for the power-spectrum decomposition of microwave anisotropies as a function of the spherical harmonic index ℓ . The solid curves refer to quasars, while the dotted or dashed curves correspond to stars with a low (2%) or high (20%) normalization for the star formation efficiency.

(dotted lines), to bracket the allowed IGM metallicity range. The panels in Figure 4 show (clockwise) the total collapsed fraction of baryons available for star or quasar formation; the evolution of the average comoving flux, J_{21} at the local Lyman limit frequency, in units of 10^{-21} erg s $^{-1}$ cm $^{-2}$ Hz $^{-1}$ sr $^{-1}$; the resulting evolution of the ionized fraction of hydrogen, F_{HII} ; and the consequent damping of the CMB anisotropies. In the first two panels, we imposed $v_{\text{circ}} \geq 75$ km s $^{-1}$ at $z < z_{\text{reion}}$. The dashed and dotted curves indicate that stars ionize the IGM by a redshift $9 \lesssim z \lesssim 13$; while the solid curve shows that quasars reionize the IGM at $z \approx 11$. This result can be understood in terms of the total number of ionizing photons produced per unit halo mass; given our normalizations of the efficiencies of star and quasar black hole formation, the relative ratios of this number in the three cases are $1 \div 0.37 \div 0.1$, respectively. A comparison of our quasar and stellar template spectra shows that stars will not reionize HeII, while quasars reionize HeII at essentially the H reionization redshift. Therefore, recent claims that HeII reionization might have been observed at $z \sim 3$ [52] could rule-out the presence of mini-quasars with hard spectra extending to X-rays at high redshifts, if these claims are verified by future observations.

The X-ray background (XRB) [53,54] might provide another useful constraint on the mini-quasar models. In Figure 5 we show the predicted spectrum of the UV to the soft XRB at $z = 0$ in these models (solid lines). In computing the spectrum,

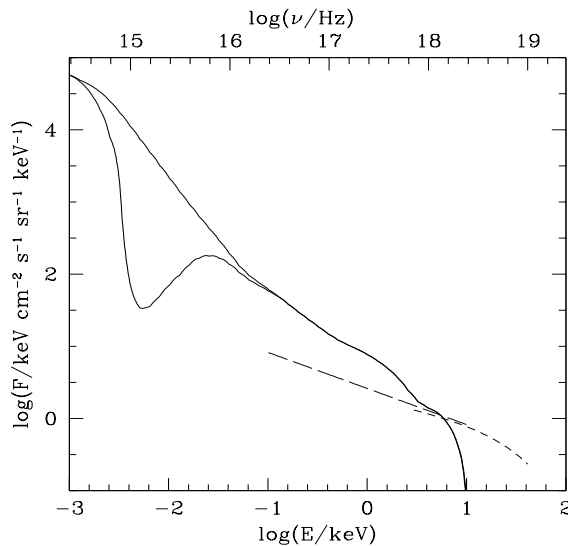


FIGURE 5. *Spectrum of the UV/X-ray background in the mini-quasar model, assuming that the median X-ray spectrum of quasars [49] is universal. The solid curves show the spectrum with and without absorption by the Ly α forest at high-redshifts. The short and long dashed lines show the unresolved fraction (assumed to be 25%) of the observed X-ray background spectrum (from [53] and [54]).*

we included absorption by neutral H and He in the IGM at $z > z_{\text{reion}} = 11$ and hydrogen absorption [55] by the (extrapolated) Ly α forest at $z \leq 11$. Also shown in this figure is the unresolved 25% fraction of the observed soft XRB [53,54]. The dashed lines in figure 5 represent an upper limit on any component of the XRB that could arise from high-redshift quasar activity. As the figure shows, the mini-quasar models overpredict the *unresolved flux* by a factor of $\sim 2-7$ in the 0.1-1 keV range, as they produce a flux comparable to the entire soft XRB flux. If an even larger fraction of the XRB will be resolved into low-redshift AGNs in the future, then the XRB could be used to place stringent constraints on the X-ray spectrum or the abundance of the mini-quasars discussed here.

CAN THE REIONIZATION REDSHIFT BE INFERRED FROM A SOURCE SPECTRUM?

The spectrum of a source at a redshift $z_s > z_{\text{reion}}$ should show a Gunn-Peterson (GP) [56] trough due to absorption by the neutral IGM at wavelengths shorter than the local Ly α resonance at the source, $\lambda_{\text{obs}} < \lambda_\alpha(1 + z_s)$. By itself, the detection of such a trough would not uniquely establish the fact that the source is located beyond z_{reion} , since the lack of any observed flux could be equally caused by: (i) ionized regions with some residual neutral fraction, (ii) individual damped Ly α absorbers, or (iii) line blanketing from lower column density Ly α forest absorbers. On the

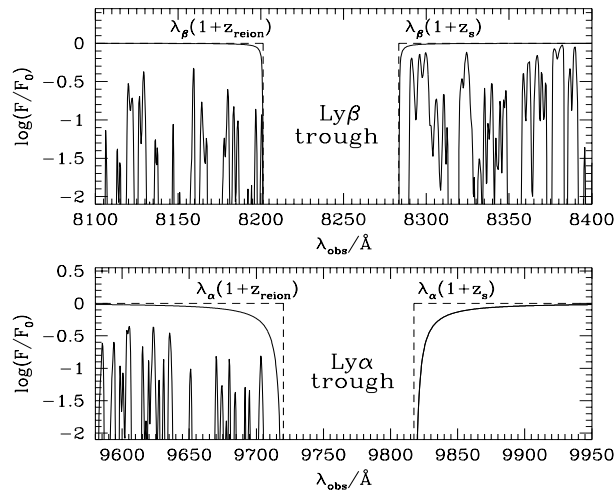


FIGURE 6. Spectrum of a source at $z_s = 7.08$, assuming sudden reionization at a redshift $z_{\text{reion}} = 7$. The solid curves show the spectrum without absorption by the high-redshift Ly α forest, and the dashed lines show the spectrum when the damping wings are also ignored.

other hand, for a source located at a redshift z_s beyond but close to reionization, $(1 + z_{\text{reion}}) < (1 + z_s) < \frac{32}{27}(1 + z_{\text{reion}})$, the GP trough splits into disjoint Lyman α , β , and possibly higher Lyman series troughs, with some transmitted flux in between these troughs. Although the transmitted flux is suppressed considerably by the dense Ly α forest after reionization, it is still detectable for sufficiently bright sources, and can be used to infer the reionization redshift.

As an example, we show in Figure 6 the simulated spectrum around the Lyman α and β GP troughs of a source at redshift $z_s = 7.08$, assuming that reionization occurs suddenly at $z_{\text{reion}} = 7$. We have included the extrapolated effects of Ly α absorbers along the lines of sight, whose statistics were chosen so as to obey the redshift dependence and absorption line characteristics of observational data at $z < 4.3$ [57]. Although the continuum flux is strongly suppressed, the spectrum contains numerous transmission features; these features are typically a few \AA wide, have a central intensity of a few percent of the underlying continuum, and are separated by $\sim 10\text{\AA}$. For sudden reionization, the nominal integration time of about 10 hours for a ~ 10 nJy sensitivity (with $\lambda/\Delta\lambda=100$ and $S/N=10$) would be sufficient to determine z_{reion} up to a redshift of ~ 7 with a high precision, by determining the location of the short-wavelength edge of the troughs shown in Figure 6. More gradual reionization would smear the edge of the GP trough. Based on the extrapolation of the Ly α forest to higher redshifts, the required sensitivity needs to be one or two orders of magnitude higher if $z_{\text{reion}} \sim 8$ or ~ 9 (see [19] for details).

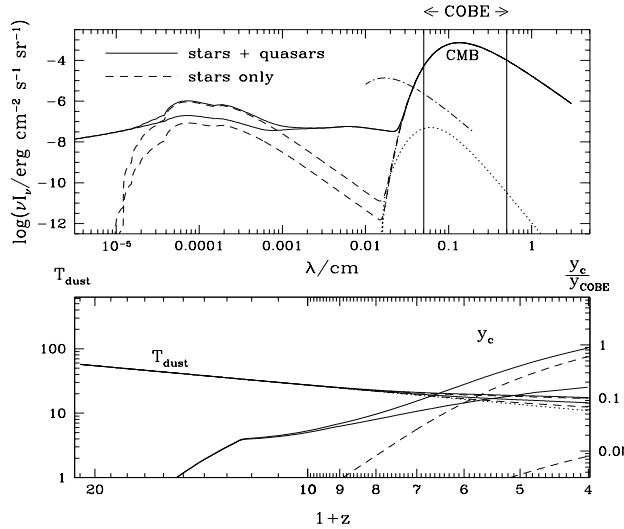


FIGURE 7. *Effect of dust on the background flux. The top panel shows the comoving spectra in four different models at $z = 3$, and the bottom panel shows the corresponding evolution of the dust temperature and Compton y -parameter (see text).*

SIGNATURES IMPRINTED ON THE CMB

The free electrons produced by the reionization of the intergalactic medium partially smooth-out the temperature anisotropies of the CMB via Thomson scattering. Given the ionized fraction of hydrogen as a function of redshift, one can readily derive the electron scattering optical depth (τ_{es}), as well as the anisotropy damping factor (R_ℓ^2), as functions of the spherical harmonic index ℓ of the multipole expansion of the anisotropies on the sky [58]. As illustrated in the lower right panel of Figure 4, the amplitude of the anisotropies is reduced by $\sim 6 - 10\%$ on scales below the angular scale of the horizon at reionization ($\ell \gtrsim 10$). Although small, this reduction is within the proposed sensitivities of the future MAP and Planck satellites, provided that both temperature and polarization anisotropy data will be gathered in these experiments (see Table 2 in [59]).

In addition, the dust that is inevitably produced by the first type II supernovae, absorbs the UV emission from early stars and quasars and re-emits this energy at longer wavelengths, where it distorts the CMB spectrum. We have calculated this spectral distortion assuming that each type II supernova yields $0.3M_\odot$ of dust with the wavelength-dependent opacity of Galactic dust [60]. We have conservatively assumed that similarly to the observed intergalactic mixing of metals, this dust gets uniformly distributed throughout the intergalactic medium. Clumpiness of the dust around UV sources would only enhance our predicted spectral distortion. The top panel of Figure 7 shows the resulting total comoving spectrum of the radiation background (CMB + direct quasar and/or stellar emission + dust emission) at $z = 3$. More distortion could be added between $0 < z < 3$ by dust and radiation

from galaxies. For reference, we also show by the dot-dashed lines the recently detected cosmic infrared background (CIB, [61]), and the typical dust peak in our calculations (dotted lines).

Figure 7 shows that in our models the dust emission peaks at a wavelength which is an order of magnitude longer than that of the CIB peak. This is a result of our assumption of a homogeneous dust distribution, and the consequent cold dust temperature. An inhomogeneous distribution of dust would raise its temperature, and could contribute significantly to the observed CIB peak. The deviation from the pure $2.728(1+z)$ K blackbody shape is quantified by the Compton y -parameter, whose redshift evolution is shown in the bottom panel. Ignoring the UV flux from quasars, we obtain $1.1 \times 10^{-7} < y_c < 8.2 \times 10^{-6}$ at $z = 3$ (dashed lines), just below the upper limit [62] set by COBE, $y < 1.5 \times 10^{-5}$. Adding the UV flux of quasars increases the y -parameter to $4.1 \times 10^{-6} < y_c < 2 \times 10^{-5}$. The distortion by the intergalactic dust may have been overestimated in our calculation as we ignored the absorption of the UV background by the neutral component of the IGM. Nevertheless, a substantial fraction (~ 10 –50%) of the total y -parameter results simply from the direct far-infrared emission by early quasars and could be present even in the absence of any intergalactic dust.

ACKNOWLEDGEMENTS

We are grateful to Martin Rees for sharing his insights during our collaboration on some of the topics described in this review. ZH acknowledges support at Fermilab by the DOE and the NASA grant NAG 5-7092.

REFERENCES

1. Rees, M. J. 1996, preprint astro-ph/9608196
2. Loeb, A. 1998, in Proc. of 34th Liege International Astrophysics Colloquium on the "Next Generation Space Telescope", Belgium, June 1998, preprint astro-ph/9806163
3. Hu, E. M., Cowie, L. L., & McMahon, R. G. 1998, ApJ, 502, L99
4. Dey, A., Spinrad, H., Stern, D., Graham, J. R., & Chaffee, F. H. 1998, ApJ, 498, L93
5. Miralda-Escudé, J. 1998, ApJ, 501, 15
6. Haiman, Z., & Spaans, M. 1998, ApJ, submitted, astro-ph/9809223, see also this proceedings.
7. Carr, B. J., Bond, J. R., & Arnett, W. D. 1984, ApJ, 277, 445
8. Wright, E. L. 1981, ApJ, 250, 1
9. Press, W. H., & Schechter, P. L. 1974, ApJ, 181, 425
10. Tytler, D. *et al.* 1995, in *QSO Absorption Lines*, ed. G. Meylan ed., Springer, p.289
11. Songaila, A., & Cowie, L. L. 1996, AJ, 112, 335
12. Pei, Y. C. 1995, ApJ, 438, 623
13. Ostriker, J. P., & Steinhardt, P. J. 1995, Nature, 377, 600

14. Haiman, Z., Thoul, A., & Loeb, A. 1996, ApJ, 464, 523
15. Haiman, Z., & Loeb, A. 1997a, ApJ, 483, 21
16. Haiman, Z., & Loeb, A. 1997b, in Proceedings of *Science with the Next Generation Space Telescope*, eds. E. Smith & A. Koratkar
17. Loeb, A., & Haiman, Z. 1997, ApJ, 490, 571
18. Haiman, Z., & Loeb, A. 1998a, ApJ, 503, 505
19. Haiman, Z., & Loeb, A. 1998b, ApJ, in press, preprint astro-ph/9807070
20. Haiman, Z., Madau, P., & Loeb, A. 1999, ApJ, in press, preprint astro-ph/9805258
21. Abel, T., Bryan, G., & Norman, M. T. 1998, in proceedings of *Evolution of Large Scale Structure*, Garching, Germany, preprint astro-ph/9810215
22. Gnedin, N. Y., & Ostriker, J. P. 1997, ApJ, 486, 581
23. Bertschinger, E. 1985, ApJS, 58, 39
24. Saslaw, W.C., & Zipoy, D. 1967, Nature, 216, 976
25. Stecher, T. P., & Williams, D. A. 1967, ApJ, 149, L29
26. Haiman, Z., Rees, M. J. R., & Loeb, A. 1997, ApJ, 476, 458
27. Doroshkevich, A.G., Zel'dovich, Ya. B., & Novikov, I. D. 1967, Sov. Astr. A. J., 11, 233.
28. Couchman, H. M. P. & Rees, M. J. 1986, MNRAS, 221, 53
29. Songaila, A. 1997, ApJL, 490, 1
30. Scalo, J. M. 1986, Fund. Cosm. Phys., 11, 1
31. Renzini, A., & Voli, M. 1981, A&A, 94, 175
32. Norman, M. L. 1998, this proceedings
33. Kormendy, J., Bender, R., Magorrian, J., Tremaine, S., Gebhardt, K., Richstone, D., Dressler, A., Faber, S. M., Grillmair, C., & Lauer, T. R. 1997, ApJL, 482, 139
34. Magorrian, J., *et al.* 1998, A&A, 115, 2285
35. van der Marel, R. P. 1998, AJ, in press, astro-ph/9806365
36. Haehnelt, M. G., Natarajan, P., & Rees, M. J. 1998, preprint astro-ph/9712259
37. Eisenstein, D. J., & Loeb, A. 1995, ApJ, 443, 11
38. Loeb, A. 1997, in Proceedings of *Science with the Next Generation Space Telescope*, eds. E. Smith & A. Koratkar, pp. 73-86, astro-ph/9704290
39. see <http://www.ngst.nasa.gov>
40. Miralda-Escudé, J., & Rees, M. J. 1997, ApJ, 478, L57
41. Woods, E., & Loeb, A. 1998, ApJ, in press, preprint astro-ph/9803249
42. Madau, P., Ferguson, H. C., Dickinson, M. E., Giavalisco, M., Steidel, C. C., & Fruchter, A. 1996, MNRAS, 283, 1388
43. Baugh, C. M., Cole, S., Frenk, C. S. & Lacey, C. G. 1998, ApJ, 498, 504
44. Conti, A., Kennefick, J. D., Martini, P., & Osmer, P. S. 1999, AJ, in press, astro-ph/9808020
45. Thoul, A. A., & Weinberg, D. H. 1996, ApJ, 465, 608
46. Navarro, J. F., & Steinmetz, M. 1997, ApJ, 478, 13
47. Jarvis, R. M., & MacAlpine, G. M. 1998, AJ, in press, preprint astro-ph/9810491
48. Thompson, R., *et al.* 1998, astro-ph/9810285, see also this proceedings
49. Elvis, M., Wilkes, B. J., McDowell, J. C., Green, R. F., Bechtold, J., Willner, S. P., Oey, M. S., Polowski, E., & Cutri, R. 1994, ApJS, 95, 1
50. Kurucz, R., CD-ROM No. 13, ATLAS9 Stellar Atmosphere Programs (1993)

FIRST STARS AND QUASARS

51. Schaller, G., Schaerer, D., Meynet, G., & Maeder, A. 1992, *A&AS*, 96, 269
52. Reimers, D., Köhler, S., Wisotzki, L., Grootte, D., Rodriguez-Pascual, P., & Wamsteker, W. 1997, *A&A*, 326, 489
53. Miyaji, T., Ishisaki, Y., Ogasaka, Y., Ueda Y., Freyberg, M. J., Hasinger, G., & Tanaka, Y. 1998, *A&A* 334, L13
54. Fabian, A. C. & Barcons, X. 1992, *ARA&A*, 30, 429
55. Madau, P. 1996, *ApJ*, 441, 18
56. Gunn, J. E., & Peterson, B. A. 1965, *ApJ*, 142, 1633
57. Fardal, M. A., Giroux, M. L., & Shull, J. M. 1998, *AJ*, 115, 2206
58. Hu, W., & White, M. 1997, *ApJ*, 479, 568
59. Zaldarriaga, M., Spergel, D., & Seljak, U. 1997, *ApJ*, 488, 1
60. Mathis, J. S. 1990, *ARA&A*, 28, 37
61. Hauser, M. G. 1997, *ApJ*, in press, astro-ph/9806167
62. Fixsen, D. J., Cheng, E. S., Gales, J. M., Mather, J. C., Shafer, R. A., & Wright, E. L. 1996, *ApJ*, 473, 576